Calculation of the ultracold neutron upscattering loss probability in fluid walled storage bottles using experimental measurements of the liquid thermomechanical properties of fomblin

S. K. Lamoreaux
University of California, Los Alamos National Laboratory, Physics Division P-23, Los Alamos, New Mexico 87545

R. Golub
Hahn-Meitner Institut, Gleinicker Str. 100, D-14109 Berlin, Germany

(Received 5 April 2002; published 28 October 2002)

Presently, the most accurate values of the free neutron beta-decay lifetime result from measurements using fluid-coated ultacold neutron (UCN) storage bottles. The purpose of this work is to investigate the temperature-dependent UCN loss rate from these storage systems. To verify that the surface properites of fomblin films are the same as the bulk properties, we present experimental measurements of the properties of a liquid ''fomblin'' surface obtained by the quasielastic scattering of laser light. The properties include the surface tension and viscosity as functions of temperature. The results are compared to measurements of the bulk fluid properties. We then calculate the upscattering rate of UCNs from thermally excited surface capillary waves on the liquid surface and compare the results to experimental measurements of the UCN lifetime in fomblin-fluid-walled UCN storage bottles, and show that the excess storage loss rate for UCN energies near the fomblin potential can be explained. The rapid temperature dependence of the fomblin storage lifetime is explained by our analysis.

DOI: 10.1103/PhysRevC.66.044309 PACS number(s): 14.20.Dh, 61.12.−q, 03.75.−b

I. INTRODUCTION

The concept of a fluid-walled ultracold neutron (UCN) storage bottle is due to Bates [1] who developed and demonstrated the technique at the Risley reactor in the U.K. The basic idea is that a hydrogen-free fluorinated oil (fomblin) wets glass and metal surfaces, and thereby produces a clean, chemically perfect, microscopically flat, and reproducible UCN reflecting surface. Fomblin is quite viscous at room temperature; when it is sprayed onto surfaces, it drains away, leaving a thin stable film. The fluid readily seals gaps and holes associated with UCN entrance and exit valves, provided that the mechanical parts fit rather closely. Fomblin also has a very low vapor pressure. Some of the most accurate determinations of the neutron β-decay lifetime have been obtained with fomblin-walled storage cells [2,3].

There is some uncertainty in the chemical formula of fomblin Y Vac 18/8 (manufactured by Ausimont/Montedison Group), the material most widely used in UCN storage experiments. The mean molecular weight is 2650, and the stoichiometry is roughly C_3F_6O, with density at 20 °C of 1.89 g/cm^3, with a mean effective UCN potential of $V = 106.5$ neV. The UCN loss coefficient [[4], Eq. (2.66)] is given by the ratio of the imaginary W to real part V of the effective UCN potential,

$$f = \frac{W}{V} = \frac{\sigma_l k}{4\pi a},$$

where σ_l is the total $1/v$ loss cross section for neutrons with wave number k, and a is the coherent scattering length. f has contributions from nuclear absorption and bulk processes, e.g., upscattering which occurs for temperature $T>0$. For the range of formulas for fomblin given in [5], the possible values of f due to nuclear absorption lie in the range

$$2.5\times10^{-7} < f < 6\times10^{-7}. \quad (1)$$

The uncertainty in the fomblin molecular formula given in [5] is a result of the coherent scattering lengths of C, F, and O being quite similar (6.65, 5.60, and 5.81 fm, respectively) so the effective UCN potential V is relatively insensitive to the relative numbers of each atomic species. On the other hand, the nuclear absorption cross sections of C, F, and O are quite different [3.5, 9.6 ± 0.5, and 0.19 mb, respectively, for thermal (2200 m/s) neutrons]. Thus, the stoichiometry of fomblin could be better determined by simultaneously considering f extrapolated to $T=0$, which is quite sensitive to the atomic fraction of F because it has a comparatively larger absorption cross section, and V, which cannot be used to effectively determine the relative amounts of F and O.

For experiments operated near room temperature (290–320 K), it is found that

$$2\times10^{-5} < f < 6\times10^{-5} \quad (2)$$

and the temperature dependence of f is much faster than being proportional to T or $\sqrt{T}$ as might be expected due to atomic and molecular fluctuations in the wall (see, e.g., [4], Sec. 2.4.6) and, in fact, seems to follow the viscosity temperature dependence rather closely. Some attempts were made to explain the observed temperature dependence of f. For example, if there is a $1/v$ cross section for slow neutrons due to upscattering in the fluid, this cross section can be used to modify W to include this loss mechanism and, in this regard, the transmission of 60 Å neutrons through a sample of fomblin as a function of sample temperature was measured [6]. These measurements are discussed in [2] where it is stated that the temperature dependence of f comes within a factor of 1.5 of explaining the experimentally observed temperature dependence of the loss rate. The loss rate for the

lowest temperature 218 K [7] implies $f=6\pm2\times10^{-6}$ which is still an order of magnitude greater than Eq. (1). More recent measurements by Morozov of the transmission of 9 m/s neutrons through a 4-mm-thick sample as a function of temperature are consistent with these results [8].

It is possible that $f(T)$ has contributions from different sources. The purpose of our work reported here is to evaluate the upscattering loss of UCN due to thermally excited surface capillary waves. Pokotilovski has investigated the energy broadening of (monochromatic) UCN stored in a fluid-walled bottle [9,10]; this is a question closely related to the upscattering loss, but it seems to us that the temperature-dependent loss rate is an experimentally better studied phenomenon but is lacking a fundamental explanation. The principal data we will address were obtained by Richardson *et al.* [11].

II. EXPERIMENTAL DETERMINATION OF THE THERMOMECHANICAL PROPERTIES OF FOMBLIN Y Vac 18/8

Although the properties of this material are available from the manufacturer, we thought it prudent to perform measurements ourselves under conditions similar to those used in an experiment. The sample of fomblin Y Vac 18/8 (hereafter referred to as fomblin) was obtained from that used in [2]. There is anecdotal evidence that the viscosity changes for degassed samples in vacuum compared to samples that have been stored a long time in air. We therefore performed our measurements with the fomblin under vacuum when possible, with the material being introduced into the various apparatuses to be discussed by distillation under high vacuum ($P<5\times10^{-7}$ torr).

These measurements were done in August 1991; some details were lost (e.g., specific equipment models employed), but given the modest accuracy of the results, these details are not important.

A. Mechanical viscosity measurement

The viscosity was determined by the time it took for a known volume of fomblin to drain through a Pyrex capillary of known length and diameter, under the influence of gravity. The glass system comprising two relatively large volumes connected by a capillary is shown in Fig. 1. Marks were placed on the large tubes corresponding to a volume $v=0.425\pm0.005$ cm^3. The capillary diameter was 2.00 ± 0.01 mm, with length 4.8 ± 0.1 cm.

Fomblin was distilled into the glass measurement apparatus under high vacuum; the glass was sealed off from the vacuum system, and the time to drain the known volume was measured as a function of temperature, with the temperature determined by a water bath. The kinematic viscosity is given by [[12], Eq. (17.10)]

$$\nu=\frac{\pi g}{8(V/t)}R^4, \tag{3}$$

where ν is the kinematic viscosity, g the acceleration of gravity, V is the known volume, t is the time to drain the known volume, and R is the capillary radius. The time to drain the volume varied from about 150 s at the lowest temperatures, to about 2 s at the highest temperatures; at the lowest temperatures, the constancy and value of the temperature were the major uncertainty (±1.2 K), while at high temperatures, the timing (to 0.1 s accuracy) was the principal limitation to the accuracy. In addition, there is a small correction associated with the change in height of the liquid layer as the fomblin drains, but it is less than 5%. The results are shown in Fig. 2 and are in good agreement with, and follow the trends of, values reported by the manufacturer (1.9, 0.09, and 0.02 cm^2/s at 293, 393, and 493 K, respectively). In the range of measurements, the viscosity is adequately described to within experimental error by the following empirical formula:

$$\nu(T)=2.0\times10^7e^{-0.055T}+900T^{-3/2}, \tag{4}$$

where ν is in cm^2/s, and T is measured in K, with estimated accuracy over the temperature range 280–308 K which will be used later.

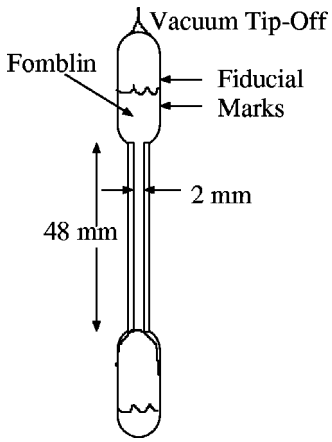

FIG. 1. Schematic of the viscosity measurement apparatus.

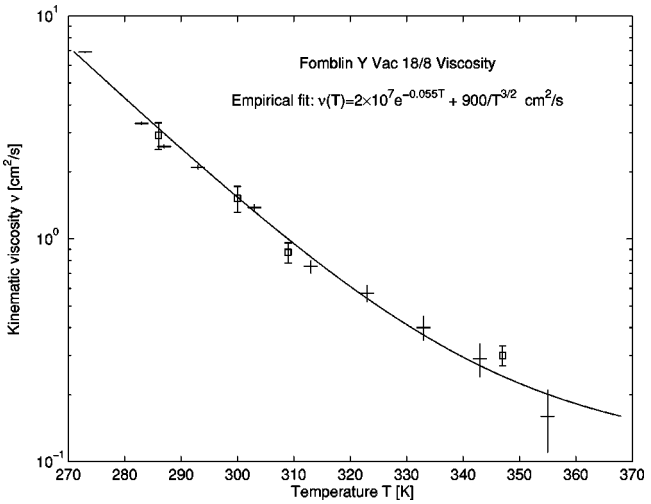

FIG. 2. Temperature dependence of the fomblin viscosity from mechanical measurements (crosses) and laser light scattering (squares).

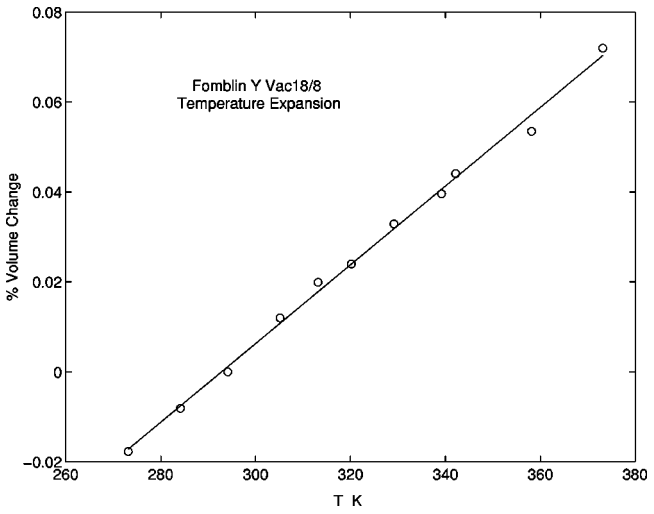

FIG. 3. Volume expansion of fomblin with temperature.

B. Thermal expansion

Fomblin was distilled into a Pyrex capillary tube of 2 mm inside diameter, filling the tube to a length of about 5 cm. The tube was sealed off from the vacuum system, and the relative change in length of the sample as a function of temperature was measured. The results are shown in Fig. 3; the principal limits to accuracy were the length measurement (± 0.2 mm) and temperature control (± 0.5 K). The thermal expansion of fomblin is about 100 times larger than Pyrex, so the expansion of the glass is an insignificant correction. The density as a function of temperature is given by

$$\rho(T) = 1.89[1 + 8.97 \times 10^{-4}(294 - T)] \text{ g/cm}^3, \qquad (5)$$

where T is measured in K, and the accuracy of this fit is about 5%. The temperature dependence of the density is particularly important because it leads directly to a temperature dependence of the effective UCN potential. This information was not available from the manufacturer.

C. Surface tension

The surface tension was measured using a Cenco student demonstration tensiometer which in essence measures the restoring force against a length of wire pulled up against the liquid surface. Unfortunately, there was no simple way to perform this measurement on a sample under vacuum. The apparatus was calibrated with de-ionized water. For fomblin, the surface tension was found to be

$$\alpha = 24 \pm 1 \quad \text{dyn/cm} \qquad (6)$$

and was independent of temperature to within measurement accuracy. The value quoted by the manufacturer is 20 dyn/cm.

D. Liquid properties by light scattering

By use of a heterodyne laser scattering technique, the dynamic liquid surface properties of fomblin could be measured directly without physically contacting the surface in any significant way. The idea is that the surface undergoes a sort of Brownian motion due to thermal fluctuations.

The theory describing the two-dimensional thermally excited surface capillary waves has been developed by Bouchiat and Meunier; when presented as time and two-dimensional surface Fourier transforms, the mean-square height fluctuations are described by [13]

$$P_{\mathbf{q}}(\omega) = P(\omega, q) = \frac{k_B T}{\pi \omega} \frac{q}{\rho} \tau^2 \text{Im}\left[\frac{1}{D(-i\omega\tau)}\right], \qquad (7)$$

where

$$D(S) = y + (1+S)^2 - \sqrt{1+2S}, \qquad (8)$$

$$y = \frac{\alpha \rho}{4 \eta^2 q}, \quad \tau = \frac{\rho}{2 \eta q^2}, \qquad (9)$$

where, as before, α is the surface tension, ρ is the density, and η is the viscosity $\eta = \nu\rho$ where ν is the kinematic viscosity.

Directed laser light reflecting from this surface will be scattered by time-varying surface disturbances, with surface wave vector q and frequency ω. By purposely aiming a fraction of the light specularly reflected from the surface in an angle corresponding to diffraction by a disturbance with wave number q (the "reference beam") to the detector, the time-dependent scattered component can be measured by beating with the reference beam. The reference beam is produced by placing a weak transmission diffraction grating in the specularly reflected beam (this grating also intercepts the scattered light which is extremely weak). This technique was proposed and developed by Hård *et al.* [14]. The specific apparatus that we used is described in [15], with the exception of the vacuum sample cell. As discussed in [15], data were acquired with the apparatus on a vibration isolated optical table. In addition, the vacuum sample cell isolated the liquid surface from disturbing air currents which were a problem for free-liquid surfaces in air.

The fomblin sample was contained under vacuum in a cubical cell; the cell was constructed of 5-mm-thick float glass plates and had internal dimension of 4 cm^3, glued together with Torr-Seal epoxy (Varian). A 5-mm-diam Pyrex tube was glued into a hole drilled in the top plate; fomblin was distilled into the cell (to a depth of 3 mm) through this tube and then sealed off from the vacuum system.

The cube was cooled/heated from the bottom with a Peltier device, and the temperature was controlled with a simple feedback loop. Light was directed onto the liquid surface at an angle of approximately 70° from normal through one of the vertical walls of the cell; the scattered and specularly reflected light exited the opposite vertical wall. The laser light was detected with a *p-i-n* photodiode, and the heterodyne signal was Fourier analyzed with a Hewlett-Packard audio frequency spectrum analyzer. Results as a function of temperature and q are shown in Fig. 4. Also shown are four-parameter fits to Eq. (7); these parameters include τ, y, an amplitude factor, and a dc offset. Results of the fits are given in Table I.

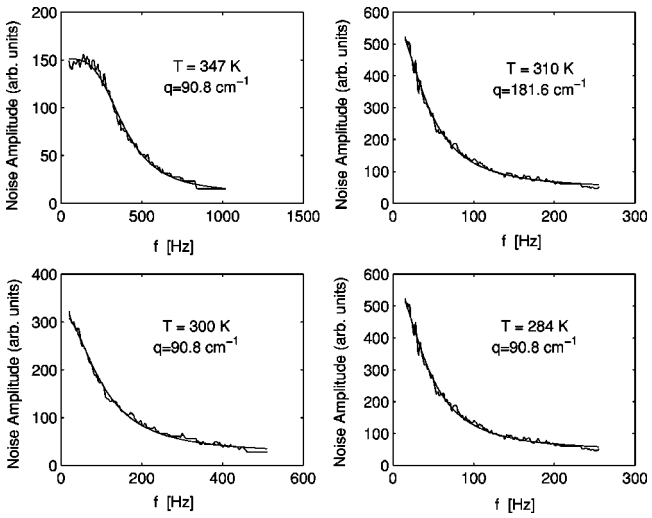

FIG. 4. Experimental measurements of heterodyne detected inelastic light scattering with theoretical fits, for various temperatures as indicated in plots.

The inferred values of ν and α are also given in in Table I. As can be seen, these results agree with previous mechanical measurements; the values of ν are plotted in Fig. 2, shown as squares.

III. CALCULATION OF THE UPSCATTERING LOSS RATE DUE TO THERMALLY EXCITED SURFACE CAPILLARY WAVES

The surface waves described in Sec. II D can inelastically scatter (diffract) a UCN that reflects from the surface. The probability to upscatter a UCN to an energy outside the UCN range can be calculated using Eq. (7) when it is properly normalized. The formalism describing nonspecular inelastic scattering was developed by Pokotilovski [10] and we will use his results with minor modifications.

A. Normalization of Eq. (7)

The work of [13] was intended to derive the spectrum of the surface fluctuations; the absolute normalization appears to have been of secondary importance. For our case, the overall magnitude is of crucial importance.

First, the static average surface distortion, based on statistical mechanics considerations, is given as

$$\overline{|\zeta_{\mathbf{q}}(0)|^2}=\frac{k_BT}{\alpha q^2\mathcal{A}}, \tag{10}$$

where $\mathcal{A}$ is the surface area. If we imagine $\mathcal{A}$ to be a square with dimensions L so $\mathcal{A}=L^2$, the effective spread in q_x and q_y is

$$\Delta q_x=\Delta q_y=\frac{2\pi}{L}\rightarrow\frac{1}{\mathcal{A}}=\frac{1}{(2\pi)^2}dq_xdq_y, \tag{11}$$

and therefore, to cast Eq. (7) per unit q_xq_y, a factor of $1/(2\pi)^2$ is required.

Second, the integral of $P(\omega,q)$ over ω should give the static result, Eq. (10):

$$\int_{-\infty}^{\infty}P(\omega,q)d\omega=\frac{k_BT}{\pi}\frac{q}{\rho}\tau^2\mathrm{Im}\int_{-\infty}^{\infty}\frac{dx}{x}\left[\frac{1}{D(-ix)}\right]$$
$$=\frac{k_BT}{\pi}\frac{q}{\rho}\tau^2\frac{\pi}{y}=\frac{k_BT}{\alpha q^2}, \tag{12}$$

where the integration was performed by noting that the only pole of the integrand is at $x=0$; by integrating along the real axis and taking a semicircle around the origin, the integral is $-i\pi$ times the residue at $x=0$ which is $1/(-iy)$.

B. Possible corrections to Eq. (7)

The coating obtained by spraying fomblin and allowing the material to drain to a thin, stable film are of order 10^{-4} cm thick or greater. The multiplicative correction factor to the capillary wave dispersion relationship, due to finite film thickness, is very roughly proportional to $\tanh(qd)$ where d is the film thickness ([12], Sec. 62, Problem 1). For q of interest for UCN scattering, 10^{-4} cm$\times q\gg 1$, so $\tanh qd\approx 1$, so we expect no significant effect due to film thickness. However, at higher temperatures where the viscosity is low, the films might drain to layers thin enough so that there is a substantial correction. The net effect will be to reduce the upscatter rate.

We are also considering rather high-frequency waves; it might be expected that the fomblin has some frequency dependence. However, fomblin appears to be a Newtonian fluid (e.g., light scattering and mechanical measurements had no anomalous behavior) and the fomblin molecules are not very large on the scale of what is considered a polymer. The molecular collisional frequency of fomblin molecules, which is one of the factors that determines the viscosity, is much higher than the frequencies of interest for UCN scattering (e.g., 10^8 Hz compared to more than 10^{10} Hz). For the analysis presented here, we will assume that the low-frequency measurements described earlier in this paper are applicable.

TABLE I. Results of fits to the data shown in Fig. 4.

T (K)	q (cm^{-1})	$2\pi\tau$ (s)	y	ν (cm^2/s)	α (dyn/cm)
286	90.8	$1.3\pm0.2\times10^{-4}$	$5\pm1\times10^{-3}$	2.9 ± 0.4	28 ± 8
300	90.8	$2.5\pm0.2\times10^{-4}$	$2.2\pm0.8\times10^{-2}$	1.52 ± 0.15	34 ± 14
309	181.6	$1.0\pm0.1\times10^{-4}$	$2.1\pm0.2\times10^{-2}$	0.87 ± 0.09	25 ± 4
347	90.8	$1.1\pm0.1\times10^{-3}$	0.32 ± 0.01	0.30 ± 0.03	26 ± 3

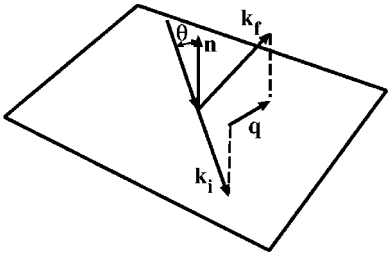

FIG. 5. Kinematics of UCN scattering from surface waves; the final energy is greater than the initial energy.

C. Kinematics

Let us consider an incident neutron with wave vector (we set the azimuthal angle of the incoming wave to zero without loss of generality); referring to Fig. 5,

$$\mathbf{k}_i = k_{ix}\hat{x} + k_{iz}\hat{z} = k_i(\sin\theta_i\hat{x} + \cos\theta_i\hat{z}), \quad k_i^2 = 2mE_i/\hbar^2, \tag{13}$$

where the polar angle θ_i is defined relative to the surface normal which is taken along $\hat{z}$, and E_i is the incident UCN energy. The surface wave disturbance can be described by

$$\mathbf{q} = q_x\hat{x} + q_y\hat{y} = q(\cos\phi_q\hat{x} + \sin\phi_q\hat{y}), \tag{14}$$

where ϕ is the azimuthal angle relative to the incident neutron momentum.

When a UCN diffracts from the time-varying surface, energy and momentum are conserved (we consider first upscattering, e.g., the UCN gains energy):

$$k_f^2 = k_i^2 + \frac{2m\omega}{\hbar}. \tag{15}$$

We can consider a UCN of specified $\mathbf{k}_i$, hence $|\mathbf{k}_i|$ is specified, and choose ω which determines $|\mathbf{k}_f|$; choosing $\mathbf{q}$ determines θ_f and ϕ_f, the polar angles of the outgoing neutron wave vector. The components of the wave vector in the liquid surface plane (denoted by subscript s) change on reflection by

$$\mathbf{k}_{fs} = \mathbf{k}_{is} + \mathbf{q} \tag{16}$$

or

$$k_{fx} = k_i\sin\theta_i + q\cos\phi, \quad k_{fy} = q\sin\phi. \tag{17}$$

For the component of $\mathbf{k}_f$ normal to the surface,

$$k_{fz}^2 = k_f^2 - k_{fx}^2 - k_{fy}^2 \geqslant 0, \tag{18}$$

where the inequality constrains the values of $\mathbf{q}$ for allowed scattering. This sets a range on the magnitude of $\mathbf{q}$:

$$0 \leqslant q \leqslant q_{max} = k_f + k_i. \tag{19}$$

In particular, we can define a kinematic factor such that

$$K(E_i, \theta_i, \omega, q, \phi) = \begin{cases} 1 & \text{if } k_{fz}^2 \geqslant 0 \\ 0 & \text{otherwise,} \end{cases} \tag{20}$$

where k_{fz}^2 is given by Eq. (18).

D. Loss probability per bounce

The probability of loss per bounce was calculated by Pokotilovski [10]:

$$w_{q,\omega_q} = 8k_{iz}k_{fz}P(\omega,q)\left|\frac{k_{iz} - iK_{iz}}{k_{fz} + iK_{fz}}\right| = 8Fk_{iz}k_{fz}P(\omega,q), \tag{21}$$

where

$$K_{i,fz}^2 = k_c^2 - k_{i,fz}^2, \tag{22}$$

with k_c the critical momentum for UCN reflection. This equation results from determining the scattered wave function amplitude then calculating the probability current normal to the surface. Pokotilovski was interested in below-barrier upscattering in which case the factor $F = 1$.

In the case where the final UCN energy is higher than the wall potential, some care must be used in calculating the upscatter loss probability. The UCN will be lost from the system if the final neutron energy is greater than the wall potential. This loss has two components: (i) The upscattered reflected wave will be lost from the system. (ii) The component of the scattered wave within the wall (film) is not an evanescent wave, but is a propagating wave [e.g., K_{fz} in Eq. (6) of [10] or Eq. (22) above is imaginary]. We must therefore account for this loss for the wave transmitted into the material. Referring to Eqs. (A6.21) and (A6.22) of [4], the amplitudes of the reflected and transmitted upscattered waves are equal. The probability current perpendicular to the liquid surface determines the loss [16]; e.g., in Eq. 21 the factor $k_{fz} \to k_{fz} + \sqrt{k_{fz}^2 - k_c^2}$. Thus,

$$F = \begin{cases} 1 & \text{if } k_{fz}^2 < k_c^2 \\ \dfrac{k_c^2}{k_{zf}[(k_{fz}^2 - k_c^2)^{1/2} + k_{fz}]} & \text{otherwise.} \end{cases} \tag{23}$$

The UCN will be lost from the system if its final energy is greater than the wall potential V. We can recast this in terms of allowed wave frequencies: For UCN loss to occur,

$$\omega + \omega_0 > \omega_c = V/\hbar, \quad \hbar\omega_0 = E_i, \tag{24}$$

where E_i is the incident UCN energy. Thus, there is a minimum ω for upscattering loss,

$$\omega_{min} = \omega_c - \omega_0. \tag{25}$$

The differential probability that a UCN, with E_i, θ_i, and ω specified, is upscattered and lost from the system due to surface waves in a small range around a value $\mathbf{q}$ is given by

$$d\mu_{sw} = 8Fk_{iz}k_{fz}w_i\frac{P(\omega,q)}{(2\pi)^2}dq_x dq_y d\omega, \tag{26}$$

where w_i is a weighting factor giving the probability for a UCN to be incident at angle θ_i,

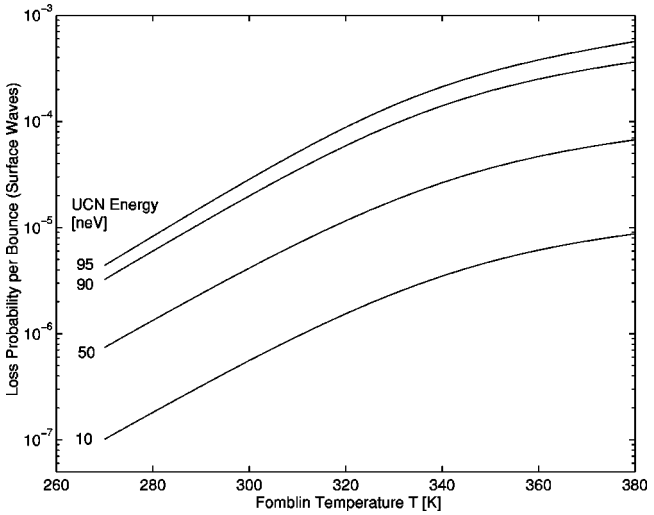

FIG. 6. Probability for UCN to upscatter to energy higher than the wall potential, as a function of temperature. Included are the temperature dependences of the viscosity and density. The effective potential is modified for the density change.

$$w_i = 2 \sin\theta_i \cos\theta_i , \tag{27}$$

and $dq_x dq_y = q dq d\phi$.

The total probability for loss is equal to the integral of $d\mu$ over q and ϕ, followed by an integration over θ_i, and finally over ω with $\omega > \omega_{min}$,

$$\mu_{sw}(E_i, T, \omega_{min}) = \int_{\omega_{min}}^{\infty} d\omega \int_0^{\pi/2} w_i d\theta_i \times \left[2 \int_0^{\pi} d\phi \int_0^{q_{max}} q dq K(E_i, \theta_i, \omega, q, \phi) \times 8 F k_{iz} k_{fz} \frac{P(\omega, q)}{(2\pi)^2} \right], \tag{28}$$

where K is defined in Eq. (20), and the dependence of μ_{sw} on the temperature (due to, e.g., the viscosity and density change of fomblin) and incident UCN energy E_i and minimum energy ω_{min} to upscatter to greater than V is explicitly indicated.

The integration is analytically unwieldy, so it has been performed numerically. The results, taking into account the temperature dependence of the viscosity and density (hence effective UCN potential) of fomblin, are shown in Fig. 6.

The slow curvature with increasing temperature (hence decreasing viscosity) results from the y term in Eq. (7), which is proportional to the surface tension, becoming important.

E. Reanalysis of previous data

It is noted in [11] that a simple fit to a value of f and to losses through holes and gaps of total area A_h does not explain the observed lifetimes of a fluid-walled bottle for energies within 10 neV of V. There is enough flexibility in f and A_h to adequately fit the lower values of energy; as seen in Fig. 6, the surface wave upscatter loss probability drops rapidly with energy. However, the temperature variation in f as derived from these fits seems nonphysical.

In general, a full Monte Carlo analysis of the system is required. For example, in a realistic storage system, the weight function, Eq. (27), becomes a function of geometry. However, 80% of the UCN loss for Eq. (28) occurs for angles between 20° and 60°, so at the 10–20 % level of accuracy, we can neglect modification of the weight function. Furthermore, a full Monte Carlo analysis would require knowledge of the liquid surface specularity for UCN reflection which is not known. Another fortunate feature of the measurements of Ref. [11] is that the cylindrical storage cell height $2R = 6.6$ cm leads to a small change in UCN energy as a function of position in the cell (7% effect) that can be modeled, as described below, with 10% accuracy.

For our reanalysis of the experimental data of Ref. [11], we use our experimentally determined values for viscosity [Eq. (4)], density [Eq. (5)], and surface tension [Eq. (6)], and neglect the uncertainties in these values. We fitted the observed lifetime versus energy data to f and A_h was done as in [11], but included all data points and the surface wave upscatter loss described by Eq. (28). However, particularly for E_i close to V, we need to take into account the effects of gravity in the storage bottle which was a horizontal cylinder with radius $R = 3.3$ cm and length $L = 160$. There are two effects that need to be accounted for. First, the upscatter loss function energy dependence is very steep for E_i approaching V. Second, a UCN that upscatters at the ''top'' of the storage vessel will gain energy as it falls and will eventually be lost from the system if the final energy $E_f \geqslant V - 2mgR$ [16]. This effect can be modeled by varying ω_{min} in Eq. (28) as a function of height in the bottle.

The total average lifetime for a UCN with initial energy E (monochromatic) specified at a horizontal plane that intersects and divides the storage vessel into two halves at the cylinder axis can be readily determined. The rate of loss can be written

$$\frac{1}{\tau(E)} = \frac{1}{\tau_\beta} + l^{-1} v(E) \overline{\mu}_{tot}(E), \tag{29}$$

where τ_β is the neutron beta-decay lifetime, l is the mean free path,

$$l^{-1} = \frac{1}{2L} + \frac{1}{2R}, \tag{30}$$

$v(E)$ is magnitude of the UCN velocity at the plane, and $\overline{\mu}_{tot}(E)$ is the total loss per bounce averaged over the storage vessel walls. The height-dependent total loss is given by

$$\mu_{tot}(E, \theta) = \left[1 - \frac{mgR\cos\theta}{E} \right]^{1/2} \left[\mu(E - mgR\cos\theta) + \mu_{sw}(E - mgR\cos\theta, T, \omega_{min} - 2mgR\cos\theta) + \frac{A_h}{4V_b} \right], \tag{31}$$

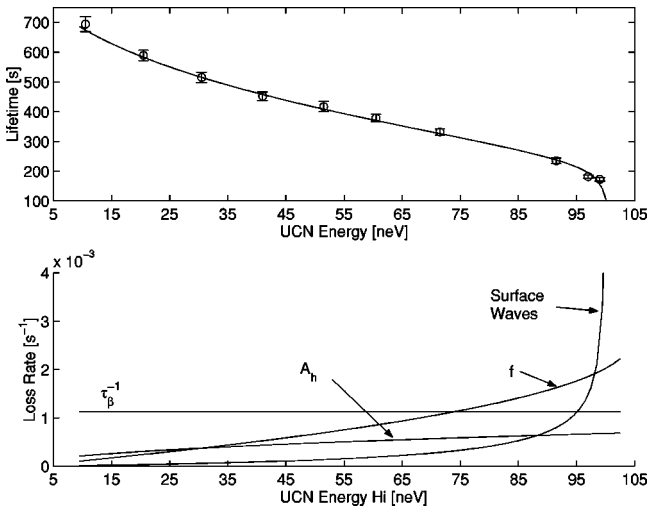

FIG. 7. Least squares fit to 294 K data from [11]. The experimentally determined values $\rho=1.89$ g/cm^3, $\nu=2.0$ cm^2/s, and $\alpha=24$ dyn/cm^2 were used in the fit to A_h and f, resulting in a reduced $\chi^2=2.1$ for the fit. The upper plot shows the net lifetime, while the lower plot shows the contributions from the various loss mechanisms.

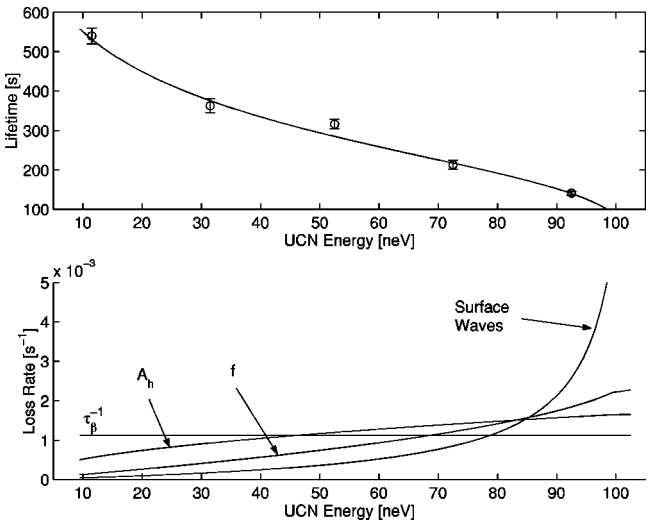

FIG. 8. Least squares fit to 308 K data from [11]. The experimentally determined values $\rho=1.87$ g/cm^3, $\nu=1.0$ cm^2/s, and $\alpha=24$ dyn/cm^2 were used in the fit to A_h and f, resulting in a reduced $\chi^2=2.4$ for the fit. The upper plot shows the net lifetime, while the lower plot shows the contributions to the loss rate from the various mechanisms.

where θ is the cylinder polar angle with $\theta=0$ being the bottom of the storage vessel, and $\mu(E)$ is the $1/v$ material loss term [[4], Eq. (2.70)],

$$\mu(E)=2f\left[\frac{V}{E}\arcsin\left(\frac{E}{V}\right)^{1/2}-\left(\frac{V}{E}-1\right)^{1/2}\right]. \tag{32}$$

As described in the Introduction, f has contributions from both nuclear absorption and upscattering and represents the losses from the UCN evanescent wave within the film during the time of reflection.

The first factor in Eq. (31) expresses the change in wall collision frequency as a function of height and has a 2% effect for $E\approx V$. The average of the storage walls is given by

$$\overline{\mu}_{tot}(E)=\frac{1}{\pi}\int_0^{\pi}\mu_{tot}(E,\theta)d\theta. \tag{33}$$

This average was numerically computed and then averaged over with the the energy resolution function given in [11], Eq. (10), to produce total loss curves as a function of temperature T; f and A_h are left as fit parameters for a given T.

The most extensive data presented in [11] are for the temperature $T=294$ K. Including the surface wave upscattering loss and fitting to the two parameters results in an excellent fit, as shown in Fig. 7. The decrease in χ^2 (see Table II) compared with the fit results presented in [11] shows the importance of the surface wave loss for UCN energies near the wall potential. It should be noted that the excess loss is not associated with slow heating of the UCN, as suggested in [11], but with a direct upscattering loss. As will be shown in the next section, the heating/cooling effect probably does not alter the functional form shown in Fig. 7.

Fits to the 283 K and 308 K data are shown in Figs. 8 and 9, with fit results tabulated in Table II. Again, including the surface wave upscattering loss provides an explanation of the extra loss rate for the higher-energy UCN.

It should be noted that the χ^2 for these fits is extremely sensitive to the energy; e.g., changing the energy for either of the two highest points in Fig. 7 by ± 1 neV changes χ^2 by a factor of 0.5– 2. Therefore, the fact that the spectrum shape can be varying during storage might be evident in the data and analysis, but as can be seen by directly considering Figs. 7–9, the simple analysis presented here is adequate to within

TABLE II. Comparison of UCN lifetime fit results without surface wave loss [9] to results using the surface wave upscattering probability given in Sec. III E. In both cases, the numbers of fit parameters are the same (2, f, and A_h). The results from [9] do not include the higher-energy lifetime data points; χ^2 given in [9] has been adjusted here to include all points (those near 100 neV were excluded from the fit in [9]).

	Ref. [9] fit results			With surface waves		
Temp (K)	f (10^{-5})	A_h (mm^2)	χ^2 (DOF)	f (10^{-5})	A_h (mm^2)	χ^2 (DOF)
283	1.9(0.2)	3.0(0.5)	5(4)	0.83(0.10)	5.6(0.5)	1.5(5)
294	2.45(0.1)	0.0(0.0)	8(8)	1.28(0.10)	3.5(0.6)	2.1(8)
308	3.9(0.5)	3.4(1.5)	9(2)	1.42(0.3)	8.3(1.0)	2.4(3)

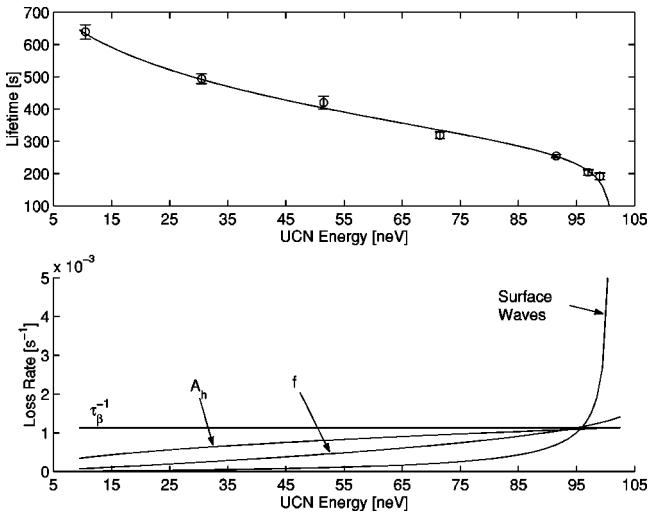

FIG. 9. Least squares fit to 283 K data from [11]. The experimentally determined values $\rho=1.91$ g/cm^3, $\nu=3.0$ cm^2/s, and $\alpha=24$ dyn/cm^2 were used in the fit to A_h and f, resulting in a reduced $\chi^2=1.5$ for the fit. The upper plot shows the net lifetime, while the lower plot shows the contribution to the loss rate from the various mechanisms.

statistics, implying an accuracy of 10–20 %. Including the uncertainties in the measured fomblin properties would lead to a modest reduction in χ^2.

Finally, the values of f for the various temperatures shown in Table II indicate a significant temperature dependence. These values, along with the value derived from [7] discussed in the Introduction, are plotted in Fig. 10. It can be seen that a crude extrapolation to $T=0$ implies a reasonable range of values for the residual (nuclear absorption) loss.

The observed variation of bottle lifetime as a function of temperature is about 4 s/K [2]; referring to Fig. 7, the contribution to the loss rate from Eq. (32) is about a factor of 2 larger than the surface wave loss rate for 70 neV UCN. Interpolating from Fig. 6, the change in μ_{sw} is about 5×10^{-8}/K for 70 neV with the fomblin near room temperature, while from Table II, f varies as $df/dT=2.3\pm1\times10^{-7}$/K. The variation in τ with change loss rate(s) can be estimated from Eqs. (27) and (30) (the effect due to the change in the potential V from thermal expansion is negligible),

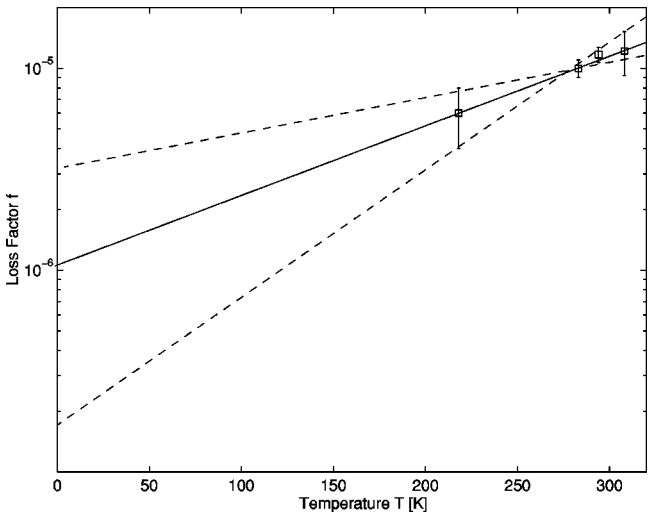

FIG. 10. Loss factor from the surface wave least squares fits (column 5 in Table II) and the 218 K value derived from [7] plotted as a function of temperature. A simple extrapolation to $T=0$ yields a range of f consistent with the nuclear absorption value.

$$\delta\tau/\delta T=\tau^2\delta\mu_{tot}/\delta T=\tau^2\frac{v}{l}[1.44\delta f+\delta\mu_{sw}]/\delta T, \quad (34)$$

which, for a 20 cm mean free path for 70 neV neutrons, with a storage lifetime of 710 s [2], implies

$$\delta\tau/\delta T=(710\ \text{s})^2[1.44\times(2.3\pm1)\times10^{-7}+5\times10^{-8}]\frac{370\ \text{cm/s}}{20\ \text{cm}}/\delta T$$
$$=3.6\pm1.6\ \text{s/K}, \quad (35)$$

which is in good agreement with 4 s/K. The surface wave loss amounts to 20% of the net total loss for 70 neV UCN at $T=294$ K. In [2], it is stated that the observed upscatter loss in the transmission of 60 Å neutrons comes within a factor of 1.5 of explaining the observed loss. Within the approximations here, it would seem that the surface wave scattering can account for most of the excess loss observed in this storage experiment.

F. UCN heating

Heating of UCN occurs when energy is gained as before, but when the final energy is still lower than the wall potential. The calculation is carried out by integrating from near $\omega=0$ to ω_{min} as defined in relation to Eq. (28). The lower limit is set by the resolution of the measurement apparatus or, e.g., by the spectral width of the stored nearly monochromatic UCN, taken here as ±2 neV, so $E_r=2$ neV and $\omega_r=E_r/\hbar$. The heating probability is thus obtained by modifying Eq. (28) [e.g., the integration over ω is not performed to get $\mu_{sq}(E_i,T,\omega)$]:

$$P_{heat}(E_i,T,\omega_r)=\int_{\omega_r}^{\omega_{min}}\mu_{sw}(E_i,T,\omega)d\omega, \quad (36)$$

where ω_{min} was defined in relation to Eq. (28) and in this case represents the maximum energy change that a UCN can receive and remain trapped. The average energy change is given by

$$\Delta\overline{E}(E_i,T,\omega_r)=\int_{\omega_r}^{\omega_{min}}\hbar\omega\mu_{sw}(E_i,T,\omega)d\omega/P_{heat}(E_i,T,\omega_r). \quad (37)$$

It is suggested in [11] that energy might be transferred to the UCN at a rate of order $\delta E_{rms}=2(1.5)\times10^{-11}$ eV per collision. The numerical results shown in Fig. 11 imply an energy change of around 10^{-13} eV per collision, obtained by taking the upscatter probability times the energy change. Of course, very small energy changes (less than the instrumental resolution) are more probable, but many more reflections are

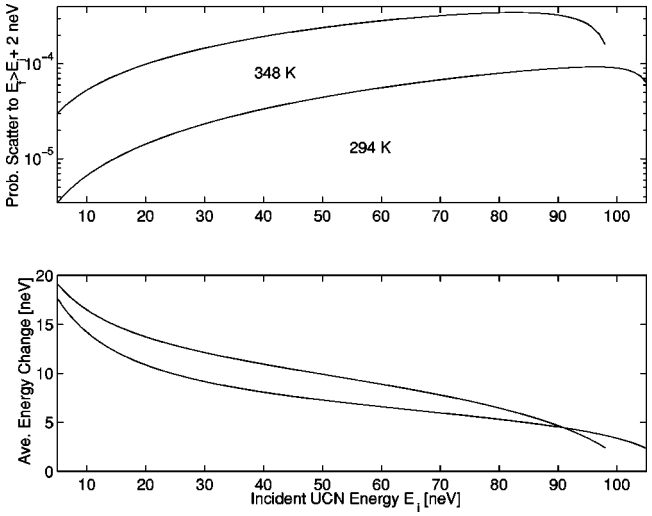

FIG. 11. Upscatter heating probability, with final energy 2 neV greater than the initial energy. Lower plot, the average change in energy with upscattering.

needed to move a UCN from the initial energy distribution; the 10^{-13} eV/collision provides a reasonable estimate of the heating rate. This result is in agreement with the results of Pokotilovski [9,10] and we thus do not further elaborate the heating issue which is more fully discussed by him.

More recent measurements by Bondarenko *et al.* [17] indicate the heating probabilities shown in Table III. In this experiment, UCN in a 0–52 neV energy range were stored in a fomblin-coated bottle, and upscattering to energies between 52 and 106 neV was detected. To calculate this probability, we assume an initial UCN energies in the 0–52 neV range and calculate the total probabilities to scatter to the 52–106 neV range using Eq. (36). The energy-dependent upscatter probabilities are then averaged over the initial spectrum presented in [17], Fig. 5. As presented in Table III, it can be seen that our results are in reasonable agreement with the experimental results, to within the reported factor of 2–3 uncertainty associated with the neutron transport efficiency in the experimental apparatus. A plot of the upscatter probability as a function of temperature, for the parameters of this experiment, is shown in Fig. 12.

The cooling rate and average energy decrease can be calculated in a similar fashion. In this case, the integration limits of Eq. (36) are 0 and $E_i/\hbar-\omega_r$. The probability to upscatter or downscatter is shown in Fig. 13. As discussed by Pokotilovski, the functions are very symmetric about the incident UCN energy, so the effects of a small energy change, either an increase or a decrease, tend to be averaged away.

TABLE III. Recent experimental measurements of UCN upscatter probability [15] compared with calculations.

Temp (K)	Expt. upscatter prob.	Calc. prob.
343	$9\pm1\times10^{-6}$	2.4×10^{-5}
308	$3\pm0.8\times10^{-6}$	5.8×10^{-6}
298	$1.2\pm0.8\times10^{-6}$	3.4×10^{-6}

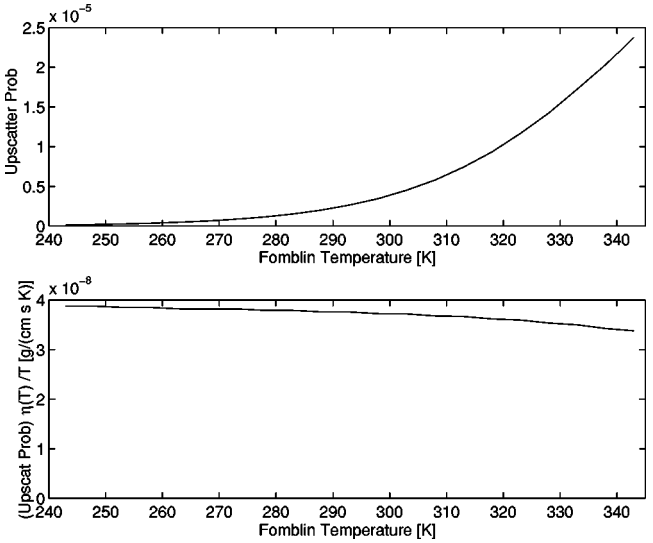

FIG. 12. Upper plot: the upscatter probability per bounce for UCN in the energy range 0–52 neV range, with initial distribution given in Fig. 5 of [17], to upscatter to the 52–106 neV energy range, as a function of fomblin temperature. Lower plot: the upscatter probability times the viscosity, divided by temperature, which is approximately constant for $T<300$ K. This is because in this temperature range the y term in Eq. (8) is relatively unimportant and $S\ll1$. This leaves Eq. (8) proportional to $T/\eta(T)$, with the integration over the q and ω factors contributing an overall factor roughly independent of T.

The measurements by Bondarenko *et al.* [17] also determined the probability for UCN with initial energy around 13 neV to downscatter to final energy in the range 0–11.5 neV and found a probability of about 10^{-6} per bounce. The temperature of the fomblin was not specified; however, the measured probability is consistent with the results presented in Fig. 13 where the integrated probability to downscatter from 10 neV initial energy to less than 8.5 neV is in the 10^{-6} range for both temperature curves shown in Fig. 13. (The

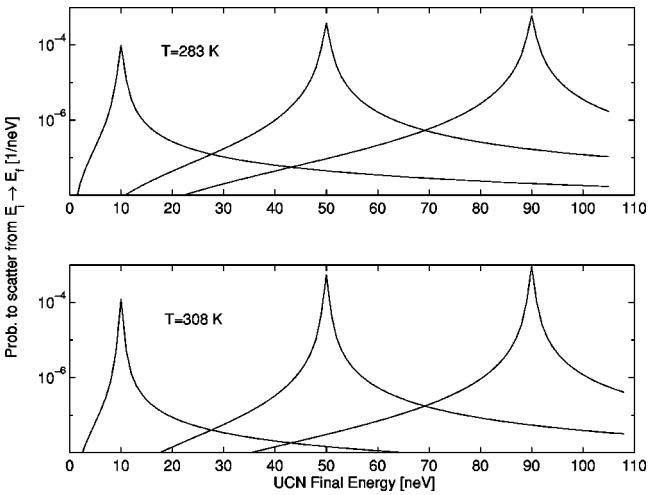

FIG. 13. The probability for UCN to upscatter or downscatter, per neV final energy, for three different UCN initial energies. These results are similar to those presented in [9,10].

variation in integrated probability with initial energy is fairly slow; the calculated result would not be significantly different for 13 neV initial energy.) The rapid drop in probability with decreasing maximum final energy that is evident in Fig. 13 is consistent, within statisitics and uncertainties in neutron transport, with the data presented in [17], Fig. 2.

IV. CONCLUSION

As shown in Figs. 7–9, the UCN lifetime for energies near 100 neV (e.g., the high-energy data points presented in Ref. [11]) are well described by upscattering loss due to surface waves. In this analysis, the low-frequency kinematic viscosity and surface tension were used. The excellent agreement between theory and experiment suggests that no modification of the low-frequency dispersion curve for the surface waves is required, but we might anticipate that for higher-accuracy data, this simple analysis ultimately might not be sufficient.

It was suggested in [11] that the excess high-energy loss is due to changes in the stored UCN spectral properties; the analysis presented here indicates that direct upscattering to energies higher than the wall potential fully account for the observed loss rate beyond that due to nuclear absorption and upscattering in the film [as parametrized by f in Eq. (32)] and losses through holes and gaps. The decrease in χ^2 for the reanalysis of the data of Richardson *et al.*, with no adjustable parameters, indicates that surface wave upscattering largely describes the excess loss rate for UCN energy close to the wall potential. As described in Sec. III F and shown in Figs. 11 and 12, the heating and cooling probabilities are sufficiently small so that, at the level of accuracy of the data presented in [11], the effects of spectral evolution are not important. However, such effects are likely important for high-accuracy determination of the neutron lifetime from fomblin-coated bottles.

We have shown that the observed temperature dependence of the net loss rate has a significant component due to the surface wave upscattering loss process. In [2], the measured temperature dependence of the lifetime for 70 neV in a fomblin-coated bottle is given as 4 s/K. This was not fully explained by the temperature dependent $1/v$ cross section [e.g., the temperature dependence of f in Eq. (32)]. The temperature-dependent loss implied by measurements of transmission of 60 Å neutrons through fomblin was 33% too small [2,6]. However, from our analysis, surface wave upscattering accounts for up to 20% of the loss for 70 neV UCN. This accounts for much of the reported discrepancy. This, together with our estimate of the temperature variation of f, explains the UCN loss in fomblin-coated bottles to within experimental errors.

Recent fomblin transmission measurements using 9 m/s neutrons by Morozov [8] indicate that $df/dT = 9 \pm 5 \times 10^{-8}$/K which is in rough agreement with the result presented in Sec. II E, based on Fig. 6. Furthermore, the values of f implied by the measurements of Ref. [8] are in agreement with the results of our analyis presented in column 5 of Table II. Unfortuantely, our value of f extrapolated to $T=0$ (Fig. 10) has too much uncertainty to help with the analysis of the fomblin stoichiometry as discussed in the Introduction.

We hope that the analysis presented here will stimulate high-accuracy experimental measurements of the temperature-dependent $1/v$ cross section of fomblin. It is our expectation that the temperature dependence of f together with the surface wave loss rate can fully explain the temperature dependence of the storage lifetime of fomblin-coated bottles.

ACKNOWLEDGMENTS

We thank Albert Steyerl for critically reading the manuscript and providing clarifications on several points. S.K.L. was supported by LANL, Grant No. LDRD-DR 2001526.

[1] J.C. Bates, Nucl. Instrum. Methods Phys. Res. A **249**, 261 (1986).
[2] W. Mampe *et al.*, Nucl. Instrum. Methods Phys. Res. A **284**, 111 (1989); Phys. Rev. Lett. **63**, 593 (1989).
[3] S. Arzumanov *et al.*, Phys. Lett. B **483**, 15 (2000).
[4] R. Golub, D. Richardson, and S.K. Lamoreaux, *Ultracold Neutrons* (Adam-Hilger, Bristol, 1991).
[5] F. Tervisidis and N. Tsaga, Nucl. Instrum. Methods Phys. Res. A **305**, 433 (1991).
[6] R. Ruddies, W. Mampe, and D. Dubbers, ''Messung der Temperaturahängigen Streuung von UCN an fomblinöl,'' Institut Laue-Langevin Praktikum, 1988 (unpublished).
[7] W. Mampe *et al.*, JETP Lett. **57**, 82 (1993).
[8] V.I. Morozov (private communication).
[9] Yu. N. Pokotilovski, Eur. Phys. J. B **8**, 1 (1999).
[10] Yu. N. Pokotilovski, Phys. Lett. A **255**, 173 (1999).
[11] D.J. Richardson *et al.*, Nucl. Instrum. Methods Phys. Res. A **308**, 568 (1991).
[12] L.D. Landau and E.M. Lifshitz, *Fluid Mechanics* (Pergamon, Oxford, 1987).
[13] M.A. Bouchiat and J. Meunier, J. Phys. (Paris) **32**, 561 (1972).
[14] S. Hård, Y. Hamnerius, and O. Nilsson, Appl. Phys. (Berlin) **47**, 2433 (1976).
[15] W.M. Klipstein, J.S. Radnich, and S.K. Lamoreaux, Am. J. Phys. **64**, 768 (1996).
[16] Albert Steyerl (private communication).
[17] L.N. Bondarenko *et al.*, Yad. Fiz. **65**, 13 (2002) [Phys. At. Nucl. **65**, 11 (2002)].